

Contact pressure distribution in guide bearings for pneumatic actuators

Original

Contact pressure distribution in guide bearings for pneumatic actuators / MANUELLO BERTETTO, Andrea; Mazza, Luigi; Pier Francesco, Orrù. - In: EXPERIMENTAL TECHNIQUES. - ISSN 1747-1567. - STAMPA. - (2015).
[10.1111/ext.12014]

Availability:

This version is available at: 11583/2511074 since:

Publisher:

SEM

Published

DOI:10.1111/ext.12014

Terms of use:

This article is made available under terms and conditions as specified in the corresponding bibliographic description in the repository

Publisher copyright

(Article begins on next page)

CONTACT PRESSURE DISTRIBUTION IN GUIDE BEARINGS FOR PNEUMATIC ACTUATORS

Andrea Manuello Bertetto^a, L. Mazza^b, P. F. Orrù^a

^a *Department of Mechanical, Chemical and Materials Engineering, Università degli Studi di*

Cagliari, Cagliari, Italy

e-mail: manuello@dimeca.unica.it

^b *Department of Mechanical and Aerospace Engineering, Politecnico di Torino*

Torino, Italy

e-mail: luigi.mazza@polito.it

ABSTRACT

This paper deals with the analysis of the contact pressure distribution at the rod/guide bearing interface of a linear pneumatic actuator. The investigation was carried out both experimentally, using pressure-sensitive film, and numerically by means of finite element analysis. By using the numerical model, it was possible to identify design changes to the cylinder front head whereby contact pressure at the bearing/rod interface can be redistributed. Operating conditions that are more advantageous in terms of wear and durability can thus be achieved.

Keywords: pneumatic cylinder, rod guide bearing, contact pressure

INTRODUCTION

Friction and wear have always had a fundamental influence on the operation of mechanical systems. In addition to being important from the mechanical standpoint, this influence is also significant economically: friction and wear cause major direct and indirect costs. In pneumatics, studies and research in this area can contribute to improving the performance and durability of components and systems featuring sliding seals and guides. Such components include the pneumatic cylinders used extensively in industrial applications for a variety of actuation purposes, where they are nominally

subjected to axial loads but, typically, can also be subject to a radial load. Radial loads arise from the weight of end-effectors mounted on the rod, i.e., grippers, weld guns, vacuum devices, video cameras, paint guns, and so forth. This load component puts significant stress on seals and guide systems, thus penalizing actuator performance in terms of durability and service life. To be able to schedule system maintenance correctly and prevent damage and machine downtime, it is important that the durability of pneumatic cylinders and actuators can be assessed in advance as a function of the main operating parameters, viz., working pressure, actuation velocity, external load and lubrication conditions.

The interest in cylinder durability and reliability extends to the normative level, as is witnessed by the many detailed standards, including international publications, covering the topic. ISO 19973-3¹ specify methods for carrying out certified life tests on commercial cylinders with radial load on the rod, analyzing collected data with an approach using Weibull statistics. This standard does not consider type of application or severity of operating conditions, nor does it cover life in service conditions. Moreover, nothing is said regarding the failure modes of damaged seals and of other cylinder sliding parts. To overcome these limitations, the major manufacturers and several research centers have investigated various methods for defining and measuring linear actuator life. A general method for evaluating pneumatic actuator service life and performance, with particular reference to sliding parts (e.g., rod guide bearing, piston slide ring and seals), was developed in Belforte et al.^{2,3}

Wear test conditions were similar to the actual service and operating conditions for a pneumatic cylinder but with a radial load higher than that contemplated by the standards, so that accelerated life tests were carried out. An extensive failure analysis and classification of damage modes made it possible to establish preventative maintenance procedures. In particular Belforte et al.⁴ established a criterion for determining actuator failure, presenting an analytical model for evaluating rod guide bearing wear and actuator life. In addition to these studies, which focused primarily on the complete cylinder, a number of analyses have addressed the guide bearing with an eye to reducing friction

and improving wear resistance. Thus, Srivastava and Pathak⁵ investigated the wear behavior and evaluated the friction coefficient of glass fiber and graphite filled epoxy resin bearings, assessing the effect of different fiber orientations and of adding solid lubricants. Marx and Junghans⁶ described a pin-on-disk type test system which can be used to evaluate friction coefficient and wear rate of different types of rod guide bearing. In particular, the effect of filling the pores of self-lubricated sintered bearings with different thermoplastics (PTFE, PEEK) was assessed. Mosleh et al.⁷ developed a model to predict the normal load increase due to the entrapment of wear particles at the sliding interface. In Menzel and Blanchet⁸ the wear resistance of PTFE and FEP samples sliding against polished steel countersurfaces is shown to be improved through the use of gamma irradiation.

The investigation described in this paper was carried out to determine and analyze the contact pressure distribution at the rod/guide bearing interface of a linear pneumatic actuator. The investigation was carried out both experimentally, using pressure-sensitive film, and numerically by means of finite element analysis. The experimental stage entailed constructing a dedicated test bench so that the pressure-sensitive film could be installed at the contact interface between guide bearing and rod. Experimental bearing/rod contact pressure distribution was identified by analyzing the imprints on the pressure-sensitive film, and then compared with the results of finite element analysis. Finally, a redesigned bearing-seat mating area is proposed in order to distribute bearing and rod contact pressure more advantageously along the bearing's axial length. By preventing contact pressure peaks and areas of concentration, this redistribution will reduce wear and increase component life.

CYLINDER UNDER TEST AND TEST SETUP

The pneumatic cylinder used in the tests is a commercial double acting cylinder as shown schematically in Figure 1.

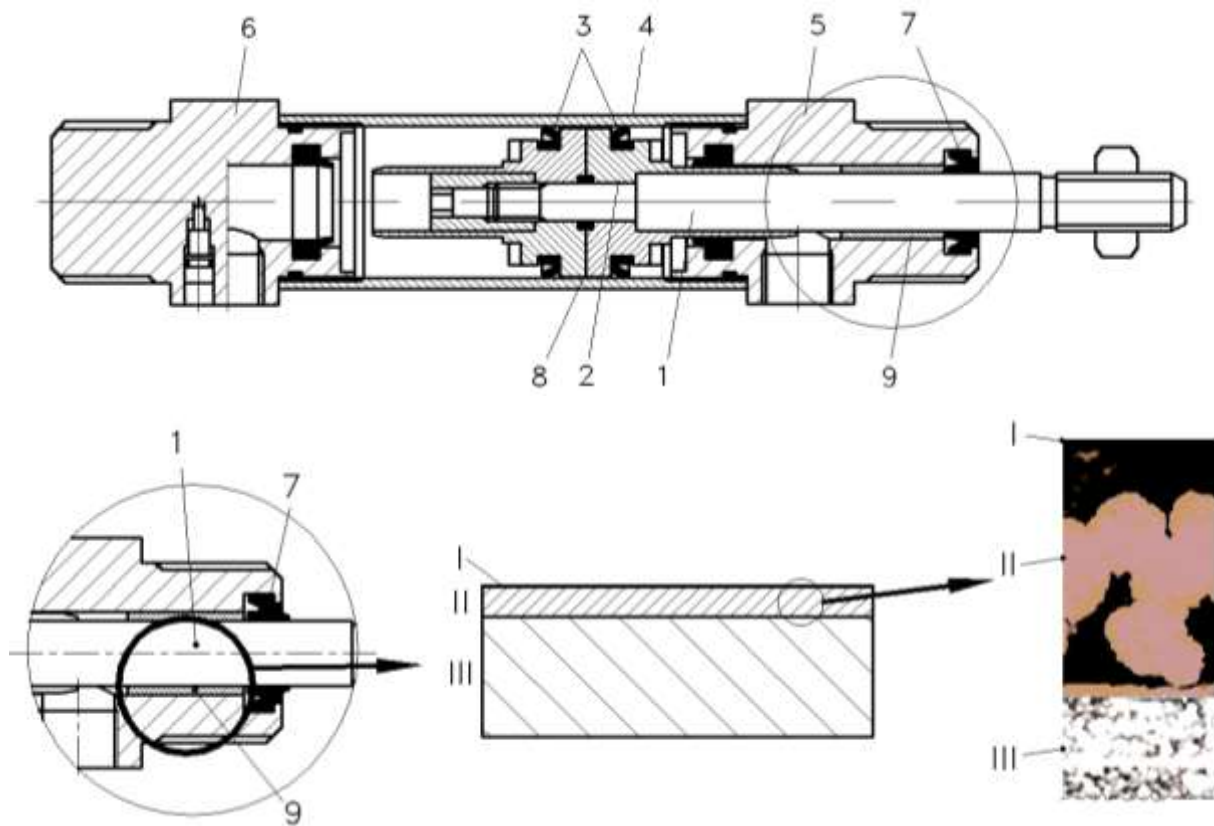


Figure 1: Cylinder schematics and guide bearing details

The rod (1) is connected to the piston (2). The piston seals (3) prevent compressed air leakage between the chambers. The cylinder bore (4) is secured between the cylinder front (5) and rear head (6). The rod seal (7) on the front head (5) is used to prevent compressed air leakage to the outside environment. Linear motion of the piston rod is guided by means of the piston slide ring (8) and the guide bearing (9). Lubricated-for-life polyurethane lip seals are used. The cylinder is a ISO 15552 series unit, working pressure 0 to 12 bar, bore 50 mm, stroke 250 mm, rod diameter 20 mm. The rod is a running fit in the guide bearing, with a clearance of approximately 5 hundredths of a mm.

Figure 1 also shows a detail of the guide bearing. The guide bearing features three bonded layers. Starting from the inside diameter in contact with the rod, these layers are: (I) a PTFE thin coating 10-30 μm thickness, (II) a porous bronze matrix impregnated with PTFE/lead (thickness about 0.25 mm), and (III), a steel backing strip (thickness about 1.25 mm). Total guide bearing radial thickness

is 1.5 mm. Rod and PTFE coating of the bearing have roughness values $R_a = 0,35 \mu\text{m}$ and $R_a = 0,61 \mu\text{m}$ respectively.

The purpose of experimental testing was to determine axial pressure distribution at the contact interface between rod and guide bearing. Cylinder loading schematics during measurement are shown in Figure 2. The cylinder is secured to a stationary frame, and a mass m is applied to the end of the rod which produces radial load Q . The rod is represented in a generic position by ' z ' and in stroke by ' s ', while force lever arms are designated as a and b . Applied load, which is entirely supported by the rod, results in constraint reactions in the guide system: R_{GB} in the rod guide bearing, and R_p in the piston slide ring. Reaction force R_{GB} determines bearing/rod contact pressure distribution which in turn causes wear on sliding parts when in relative motion.

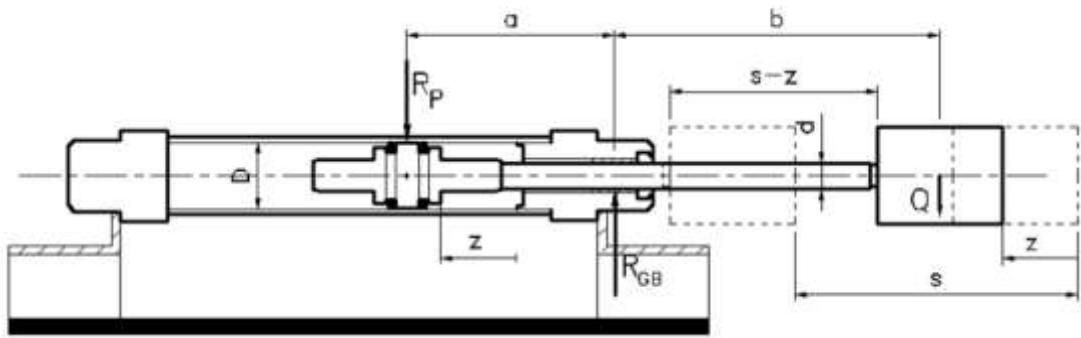


Figure 2: Cylinder loading schematics

The cylinder front head was modified in order to determine guide bearing/rod contact pressure. To do so without altering contact surface geometry, it was decided to use a contact pressure indicating sensor film produced by Fujifilm. This minimally invasive measurement instrument can be inserted between mating parts separated by very small clearances: the color density on the pressure-sensitive film's surface changes according to the intensity of the applied pressure. The sensor used in these tests consists of two matched paper-like sheets: one film is coated with a micro-encapsulated color-forming material, while the other film is coated with a color-developing material. The entire sensor

is very thin (approximately 0.2 mm). When load is applied, the microcapsules are broken, releasing the color-forming liquid which reacts with the color-developing material. As a result, red patches appear on the film whose density will vary according to the actual pressure distribution and magnitude. As there is a pressure below which no capsules will be broken, this sensor has a minimum threshold under which stresses cannot be measured. In addition, there is a pressure above which all capsules will break, which is thus a saturation threshold. Useful properties of this pressure-sensitive film include its flexibility and the fact that it can be cut to the size and shape of the surfaces whose contact pressure is to be measured. Its limitation is that each film can only be used for a single pressure reading.

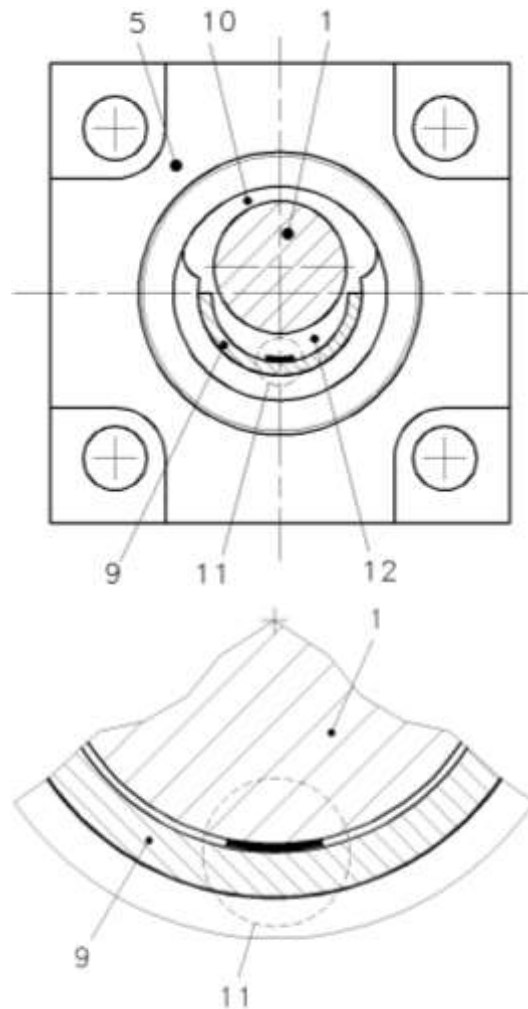


Figure 3: Schematic view of modified front head

The front head was modified so that the rod could be lifted sufficiently to insert the pressure-sensitive sheet at the guide bearing/rod contact interface. The contact pressure measurement procedure is illustrated in Figure 3. The head (5) was machined to provide a space (10) above the rod (1), while the guide bearing (9) was cut in half along a horizontal so that the rod can be lifted to insert the pressure-sensitive sheet (11) in space (12). The lower part of Figure 3 shows a detail of the measurement area: rod (1) is centered relative to the guide bearing (9), and the pressure-sensitive sheet (11) is placed in the contact zone.

Figure 4 is a photograph of the front head modified to accommodate the pressure-sensitive sheet, which can be seen at bottom center between the rod and guide bearing.



Figure 4: Modified front head with pressure-sensitive sheet inserted in contact zone

Measurement was performed using the extended pressure method, which consists of gradually reaching maximum load over a period of 2 minutes, and maintaining this load for 5 minutes. Film sensors with 0.5-2.5 MPa and 2.5-10 MPa measuring range were employed; the roughness of the pressure sensitive films is equal to $R_a=0.45\text{ }\mu\text{m}$. The output of the sensor is a data matrix with a step resolution of $125\text{ }\mu\text{m}$. In order to interpret the imprints on the sensor sheet, optical density readings must be converted into pressure values (Lee et al.⁹). To this end, the sensor sheet was calibrated using the procedure developed in (Belforte et al.¹⁰). This procedure employs a test setup in which the sensor sheet faces a chamber that can be gradually pressurized. Calibration pressure

was established by loading the sensor sheet with compressed air, thus achieving a uniform pressure distribution over the entire surface and preventing undesired edge effects.

Calibration tests were conducted at constant pressure ($t = 25^{\circ}\text{C} \pm 0.5^{\circ}\text{C}$) and 50-55% relative humidity. The measured imprint was acquired with a 24-bit scanner in order to associate a red tone with each pressure value, and the calibration curves needed to evaluate the imprints produced during experimental tests on the guide bearing were plotted. Contact pressure measurements were performed under the same environmental conditions as the calibration tests, using different masses (1, 5, 10 kg) applied to the rod with the latter fully extended ($z=0$ in Figure 2) and under static conditions (without the linear motion of the rod). The mass of 1 kg was considered as a reference for comparison between experimental and finite element results.

FINITE ELEMENT MODEL: CONTACT PRESSURE RESULTS AND COMPARISON

The fundamental factors that determine contact pressure values and distribution pattern include the geometry of the bodies in contact, the form and extent of contact, and loading and constraint conditions. Contact pressure and pressure distribution have a major influence on performance in terms of friction and durability of bodies in contact such as pneumatic cylinder seals and guide systems. There are a number of studies in which considerations regarding contact pressure against the sealing surface have served as the starting point for designing a new seal geometry or optimizing an existing geometry in order to improve tribological performance (Belforte et al.¹¹, Lee et al.¹²). In the case examined here, extended contact between the moving rod and guide bearing entails a distribution of pressure at the contact interface. This pressure gives rise to wear phenomena that lead to actuator collapse as a result of the deterioration in rod seal and guide system operating conditions. An analysis of this contact distribution could provide the basis for optimizing contact pressure patterns and thus increasing actuator life.

The guide bearing/rod system's structural behavior was investigated through a numerical finite element analysis implemented using a commercial code (Ansys Rel. 11.0). The model represents

the moving member of the actuator, coupled to the rod guide bearing housed in the cylinder front head.

Radial loads corresponding to the weights of 1, 5, 10 kg masses were applied to the free end of the rod, assembled horizontally. At the opposite end, a system of constraints was applied on the horizontal diameter so that the only degree of freedom is a rotation around the diametral axis 'y' perpendicular to the axis of the rod (Figure 5). These constraints were produced by preventing the three independent displacements of the nodes which belong to the mentioned 'y' axis. This reproduces the actual constraint on the cylinder's moving member (piston and rod) that results from its installation in the cylinder bore. The constraint between piston and the cylinder bore, in fact, is a running fit produced by the piston slide ring which, with small angular displacements as the rod flexes, is low in stiffness.

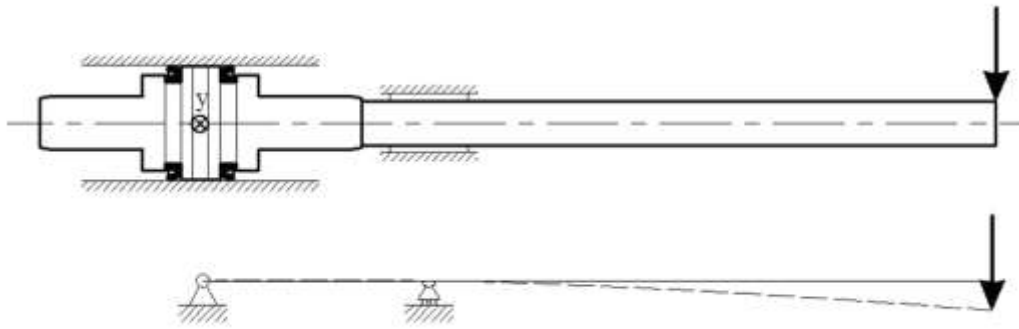


Figure 5: Constrained configuration of component

In turn, the rod is inserted in a guide bearing with a running fit that entails contact friction. As regards the constraints in the rod guide bearing, which is press-fit in the cylinder front head, all movements have been prevented at the head-bearing interface, or in other words on the outer surface of the bearing.

Figure 6 shows a detail of the model of the bearing and rod assembly, which takes advantage of the conditions of symmetry for the case in question. An increased mesh density is used at contact. The model was defined using Solid 45 8-node hexahedral elements. Average element size is approximately 1.30 mm per side, while mesh density is increased in the area where the stress gradient is believed to be higher by using approximately 0.25 mm elements. The model has a total

of 82389 degrees of freedom. Contact between bearing and rod was modelled using surface-surface Contact 170 and Target 174 elements. As constraints and loads are geometrically symmetrical with respect to the vertical plane, only one half of the structure was modelled and constraints were applied to enforce the symmetry. The bearing was modelled with a radial thickness of 0.25 mm of material consisting of a bronze alloy and PTFE, with a steel outer race having a radial thickness of 1.25mm. Material coefficients of elasticity and Poisson ratio are: $E= 210000$ MPa, $\nu=0.3$ (steel), $E= 113000$ MPa, $\nu=0.35$ (bronze). The presence of the PTFE film (whose thickness is in the order of a few hundredths of a millimeter thick) between the rod and bearing was taken into account through the contact elements' friction coefficient. Several insensitivity tests were carried out of the finite element mesh density. The mesh used is the result of a number of analyses performed in order to determine the element dimensions that do not produce significant variations in calculation precision.

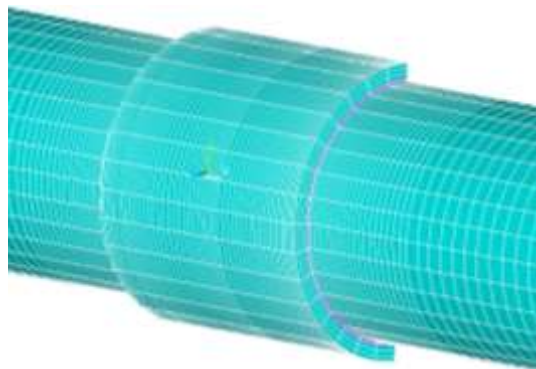


Figure 6: Detail of bearing mesh

The FE analysis was done for three different rod positions: rod fully retracted, rod at mid-stroke, and rod fully extended. To simulate actual operating conditions, in which there is a slight clearance between rod and bearing, contact at the top was eliminated. Clearance is completely taken up at the bottom contact because of the downward-acting load applied at the end of the rod, while rod deflection along the length of the bearing does not take up the clearance at the top. This phenomenon was modelled by eliminating the contact elements at the upper interface.

The analysis allowed to calculate contact pressure along the lower generating line of the rod at the interface with the bearing, and along three arcs of contact located at different axial positions. Contact pressure at the lower generating line versus bearing axial length x is plotted in the graph in Figure 7; in addition, contact pressure on a section perpendicular to the rod axis is shown versus angular position θ . Results shown in Figure 7 refer to a radial load of 10 kg mass. As can be seen from the graph, contact pressure is concentrated in a small portion of the contact surface near the extreme outer section where the contact pressure reaches its maximum. This is an undesirable operating condition, as the entire axial length of the bearing is not used to distribute contact pressure. A pattern of this kind results in areas of concentrated wear that can lead to damage, premature failure and penalizing system performance.

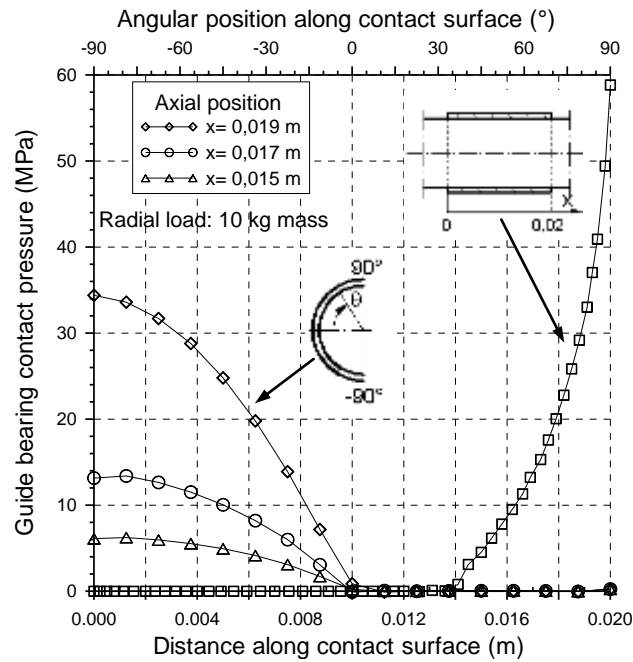


Figure 7: Contact pressure along the contact surface

Figure 8 shows a comparison between contact pressure obtained with the FEM model and that measured experimentally with the film sensor. Reference condition entails a 1 kg mass applied to the end of the rod, with the latter fully extended. By way of example, three measurement curves selected from among those plotted in the entire testing campaign with three different guide bearing samples are shown. As can be seen, measurements and numerical results are in sufficiently good

agreement. It must be pointed out that the manufacturer-specified accuracy in contact pressure levels is equal $\pm 10\%$ at 23 °C and 65% relative humidity.

It should be noted that using the film sensor needs painstaking test preparation, and also requires that the operator devote considerable effort to developing good hand skills. Great care must be taken in inserting the sensor and positioning the rod prior to load application in order to reduce the percentage of unsuccessful tests whose results must be discarded. For this reason, each test was repeated at least six times on the same guide bearing sample and under the same load conditions. Comparison of results demonstrated the validity of the proposed method, confirming that film sensor measurements are sufficiently accurate and that the finite element model is appropriate. In addition, this experimental method makes it possible to use the film sensor for monitoring purposes during the actuator's service life, as the increase in clearance between rod and guide bearing, that results from wear, may be such as to enable the sensor to be inserted between the two components. It should be noted that the stiffness of the pressure film sensor is quite lower than the stiffness of the mating parts. Because the pressure film sensor is thin this fact doesn't imply significant displacements coming from the film compliance.

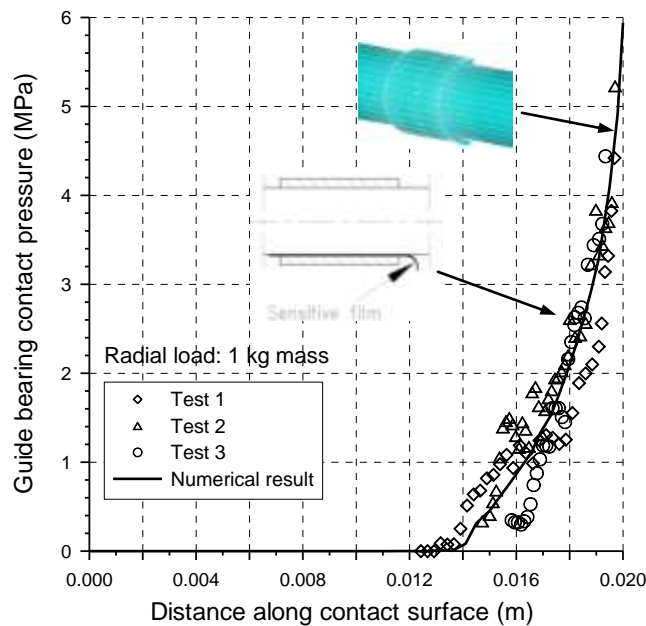


Figure 8: Contact pressure: comparison of experimental and FEM results

CONTACT PRESSURE ANALYSIS AND PROPOSED ROD GUIDE REDESIGN

The analysis of guide bearing/rod contact pressure presented above led to several proposed modifications in guide bearing geometry, material and type of constraint whose main goal was to achieve a better contact pressure distribution along the bearing's axial dimension than is provided by the analyzed commercial solution. Redistributing contact pressure to eliminate areas of concentration and reduce the pressure peak is essential in order to slow the wear process and thus lengthen the component's service life (Reye¹³). A finite element analysis approach was used for this purpose.

Figure 9 shows the five different solutions that were analyzed (A, B, C, D, E). Case A employs a bearing whose axial length is less than that of the original design. The following values were considered for ratio L/L_0 : 0.35 – 0.65 – 1. Cases B and C addressed the method whereby the bearing in the front head is constrained to the outside diameter; here, the axial length of the bearing seat is shorter than in the original design. Values for ratio L_v/L_0 of revised constraint length L_v to original constraint length L_0 are 0.35 – 0.65 – 1. Case D provides intermittent bearing constraint, with constrained zones alternating with free zones at the bearing outside diameter. Constrained and free zones are evenly divided in four equal parts ($L_N/L_0 = 0.25$). For case E, bushings have an axial length of $L = L_0$, but consist of a single material rather than being layered as in the original design. Three materials were analyzed: steel, bronze and PTFE. Case E is not illustrated in Figure 9. As can be seen, almost all of the proposed designs seek to ensure that the connection with the front head is less stiff so that the bearing can change its orientation slightly to accommodate for rod deformation under load. All bearings are designed so that they can be readily produced on standard machine tools, which simplifies prototype construction in the laboratory as well as being advantageous in the preliminary or final production processes used by pneumatic actuator manufacturers.

The following results refer to a radial load 10 kg of mass; Belforte et al. (1999) considered this load as a reference for life accelerated test.

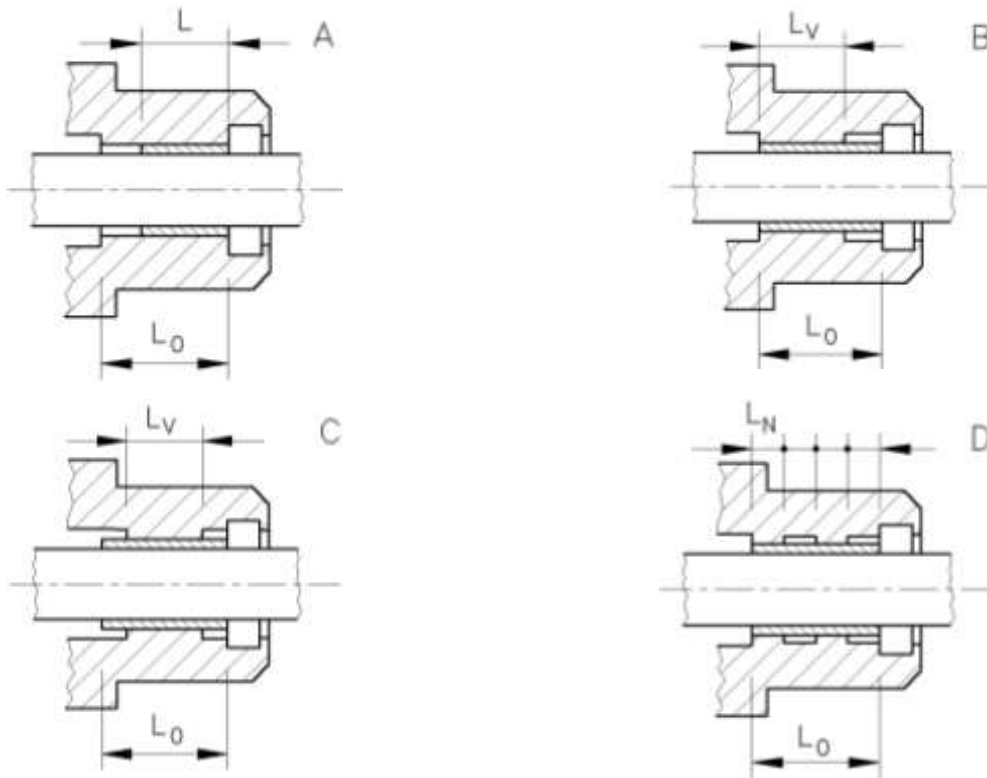


Figure 9: Guide bearing redesign, solutions under study

Figure 10 shows contact pressure along the lower generating line of contact, in the diametral plane containing the vertical load applied to the rod. Curves are given for the original bearing, the bearing with smaller axial dimensions (case A, with $L/L_0=0.35$), and the case where the bearing is constructed entirely of PTFE (case E). In case A, the contact pressure distribution curve is similar to that of the original bearing, rising sharply to a maximum level at the outermost part of the bearing. Compared to the original bearing, case A shows a higher peak pressure and a larger ratio of contact area to overall axial length. Case E with PTFE bearing shows a different pattern, as peak contact pressure is lower than contact pressure in the other cases. The pressure curve is thus smoother and shows better redistribution over the axial length.

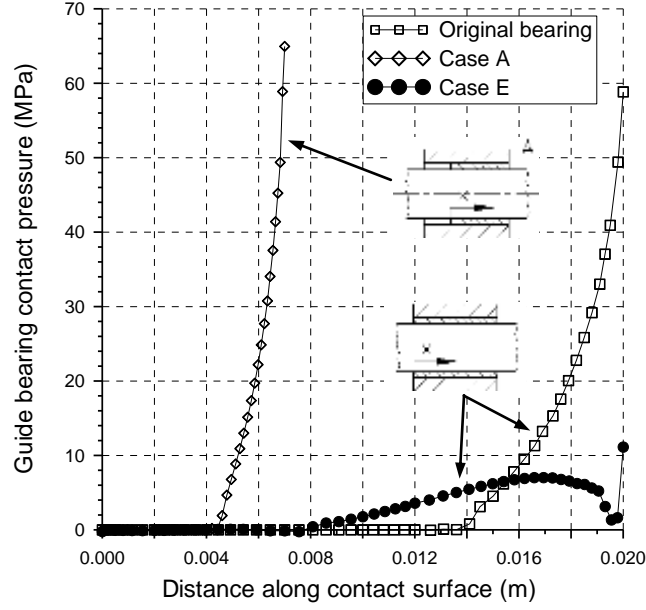


Figure 10: Guide bearing re-design, FEM contact pressure (cases A, E)

Contact pressures for the original bearing, the bearings where the axial length of the bearing seat is shorter (cases B, C, $L_v / L_0 = 0.35$), and the intermittently constrained guide bearing (case D) are shown in Figure 11. In case B, the pressure peak is approximately one-third of that of the original bearing, and occurs at the end of the bearing's axial constraint, located at a distance L_v from the origin of the abscissa. However, contact pressure is also distributed outside of the constrained zone, i.e., for axial coordinates over L_v , thus producing a greater redistribution of pressure along the contact surface. Similar considerations apply to case C. In case D, with the bearing constrained at alternating sections, the curve is similar to the previous cases, with increased pressure at the outermost constrained zone (coordinate along the upper abscissa); this means that the inner constraint zone located at a coordinate along the lower abscissa is not under load. This, unfortunately, prevents better pressure distribution along the contact surface. To improve distribution, it would be necessary to ensure that the innermost constraint zone absorbs more load, for example by using a more compliant material in this area (the head is currently constructed of aluminum).

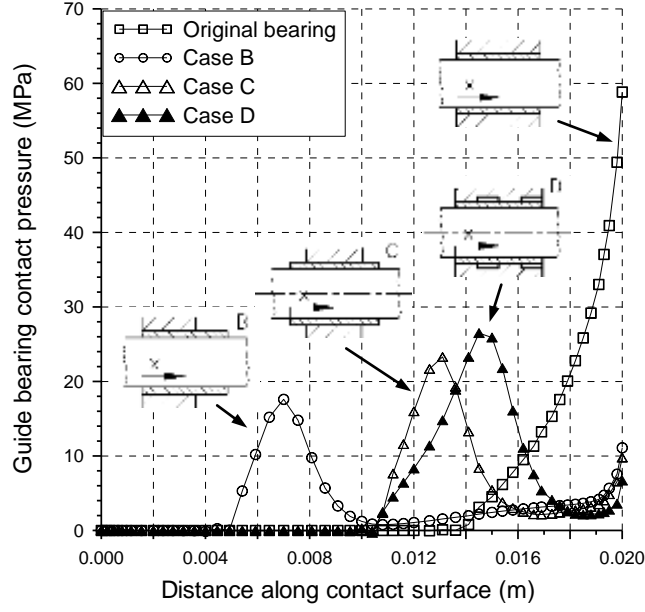


Figure 11: Guide bearing re-design, FEM contact pressure (cases B, C, D)

To evaluate how well contact pressure is distributed along the axial length, an index was defined to identify the extent to which contact pressure values are scattered around the mean. This index is the relative variation coefficient $C_v = \frac{\sigma_p}{\bar{p}}$ given by the ratio of the standard deviation σ_p of the pressure distribution to the mean value \bar{p} .

The histogram in Figure 12a shows values of coefficient C_v for each new design; higher values of this coefficient correspond to greater scatter around the mean. As can be seen from the graph, the original bearing exhibits the highest scatter of all analyzed cases; accordingly, the proposed changes to constraint conditions (cases B, C, D in Figure 9) and material (case E) make it possible to reduce coefficient C_v by an order of magnitude, and thus indicate a significant improvement in axial pressure distribution. In particular, the PTFE bearing is the best of the analyzed designs. To take the high pressures occurring in limited areas of the contact surface into account, the coefficient

$C_M = \frac{P_{MAX}}{\bar{p}}$ can be introduced; this coefficient is the ratio of maximum pressure p_{MAX} reached

over the entire contact surface to mean pressure \bar{p} . The coefficient $C_B = C_v \cdot C_M = \frac{\sigma_p}{\bar{p}} \cdot \frac{P_{MAX}}{\bar{p}}$,

which is also non-dimensional, can be regarded as indicating how good the axial contact pressure distribution is, as it takes both scatter and pressure peaks in limited areas into account. Values of coefficient C_B for the proposed designs are shown in Figure 12b.

Even though the proposed designs entail greater bearing compliance in its seat than the original component, deflection at the external load application point (rod end) does not increase significantly. For case E (PTFE bearing) in particular, deflection increases by approximately 10% over that with the original bearing.

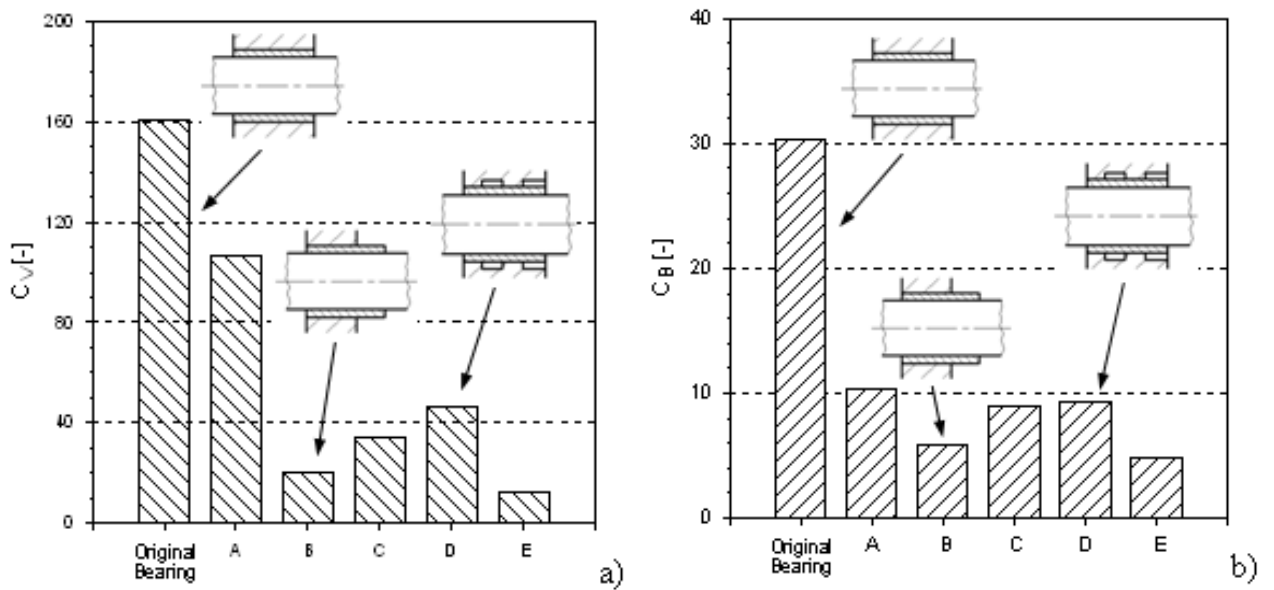


Figure 12: Guide bearing re-design, contact pressure variation coefficients

CONCLUSIONS

A finite element model and an experimental technique were developed to determine contact pressure at the guide bearing/rod interface in a pneumatic actuator; good agreement between the results obtained with the FE model and in experimental tests indicates that the proposed method of investigation and the type of testing used are valid. It was found that contact pressure distribution at the bearing/rod interface in the most common commercial components is not optimal as regards wear on guide bearings, which are critical to actuator efficiency. By using the numerical model presented in this paper, it was possible to identify design changes whereby contact pressure at the bearing/rod interface can be redistributed. All of these changes can be readily introduced in the

actuator manufacturing process. The analyses enable us to conclude that operating conditions, that are more advantageous in terms of wear and durability, can be achieved. In particular, certain design changes to the cylinder front head, which make it more adaptable to loads exerted by bearing constraints, show considerable promise for optimizing contact pressure distribution and thus minimizing wear. Preliminary life tests are now being conducted both on commercial actuators and on actuators incorporating several of the proposed changes, and appear to confirm the validity of the new designs.

ACKNOWLEDGEMENTS

This research was supported by the MIUR (Italian Ministry of Education University and Research).

REFERENCES

1. ISO 19973-3, Pneumatic Fluid Power – Assessment of component reliability by testing – Part 3: Cylinders with piston rod, (2007).
2. Belforte, G., Raparelli, T., Mazza, L., “Analysis of typical component failure situations for pneumatic cylinders under load”, *Lubr. Eng.* (48): 840-845 (1992).
3. Belforte, G., Manuello, A., Liu, S., Mazza, L., “Wear and failure analysis in pneumatic cylinders under radial load”, *Proceedings of 11th Int. Sealing Conference*, Dresden, Germany, 317-330 (1999).
4. Belforte, G., Manuello, A., Mazza, L., “Life prediction of guide bearings for linear pneumatic actuators”, *Proceedings of 2nd ECOTRIB European Congress on Tribology*, Pisa, Italy, 201-206 (2009).

5. Srivastava, V.K., Pathak, J.P., “Friction and wear properties of bushing bearing of graphite filled short glass fibre composites in dry sliding”, *Wear* (197): 145-150 (1996).
6. Marx, S., Junghans, R., “Friction and wear of highly stressed thermoplastic bearings under dry sliding conditions”, *Wear* (193), 253-260 (1996).
7. Mosleh, M., Saka, N., Suh, N.P., “A mechanism of high friction in dry sliding bearings”, *Wear* 252: 1-8 (2002).
8. Menzel, B., Blanchet, T. A., “Enhanced wear resistance of gamma-irradiated PTFE and FEP polymers and the effect of post-irradiation environmental handling”, *Wear* (258): 935-941 (2005).
9. Lee, C.Y., Lin, C.S., Jian, R.Q., Wen, C.Y., “Simulation and experimentation of the contact width and pressure distribution of lip seals”, *Trib. Int.* (39): 915–920 (2006).
10. Belforte, G., Manuello, A., Conte, M., Mazza, L., Visconte, C., “Experimental and numerical evaluation of contact pressure in pneumatic seals”, *Trib. Int.* (42): 169-175 (2009)
11. Belforte, G., Manuello, A., Mazza, L., “Optimization of the cross section of an elastomeric seal for pneumatic cylinders”, *Journal of Trib.* (128): 406–413 (2006).
12. Lee, K. O., Hur, Y. M., Kang, J. H. and Kang, S. S., “Performance estimation of dust wipers for hydraulic cylinders and optimization of geometric design variables”, *Journal of Materials Processing Technology* (187-188): 215-219 (2007).

13. Reye T., "Zur Theorie der Zapfenreibung", *Der Civilingenieur* (4): 235-255 (1860)